An Integral Analysis of Condensing Annular-Mist Flow

MAURICE R. BERRY, JR. and WILLIAM P. GOSS

Virginia Polytechnic Institute and State University, Blacksburg, Virginia

The application of integral techniques to the analysis of a high vapor velocity, two-phase, annular-mist, single-component condensing flow system is presented. A time-averaged annular liquid film thickness is defined, and appropriate interfacial and wall shear stress correlations are employed to account for the wavy nature of the interface between the entrainment-laden gaseous core and the axisymmetric annular liquid film. An empirical entrainment correlation is utilized to determine the amount of liquid flowing as entrained particles in the high velocity core region. The velocity and enthalpy distributions in the gaseous core and the annular liquid film are assumed as the power-law type. The resulting set of four nonlinear ordinary differential equations is solved numerically with the use of a digital computer. A comparison with experimental data for condensing steam is obtained. The analytical model accurately predicts the condenser length necessary for complete condensation and also predicts the dynamic quality, the heat transfer characteristics, and the static pressure distribution throughout the condensation length. The integral analysis presents some insight into the complex mechanisms and interactions which occur in high vapor velocity, two-phase, annular-mist flows and also indicates the need for improved experimental techniques to further this understanding.

Several possible flow regimes are known to exist for the flow of a liquid and vapor in a duct. These flow regimes are classified according to the spatial distribution of the two phases. One of these patterns, termed "annular-mist flow," may be described as the confined concurrent flow of a vapor and a liquid in a circular duct where a portion of the liquid flows in a low velocity annular film in contact with the duct wall, while the remainder of the liquid flows as entrained particles in a relatively high velocity gaseous core. The particular flow studied in this investigation is the condensing two-phase annular-mist flow of a single component flowing in a circular duct. Due to the cooling at the duct wall the vapor begins to condense and, for high vapor velocities and suitable wall/liquid wetting characteristics, the two-phase annular-mist pattern forms. The condensation process continues until that point where liquid flows alone in the duct. If the vapor velocity is sufficiently high enough (of the order of 500 ft/s), then the annular-mist flow regime will exist to a high degree of approximation throughout the entire condensing length. The authors have visually observed, through a short glass tube section, the annular-mist pattern up to the point of complete condensation. After the annular liquid layer fills the tube there are some entrained bubbles which exist for several tube diameters.

The design of high performance, high vapor velocity, internal flow tube condensers depends upon how accurately the two-phase pressure drop and heat transfer characteristics can be calculated. At the present time, most of the experimental data for annular-mist, two-phase flow is for two-component systems (usually air-water), while relatively little data exists for single-component systems with heat removal. Attempts at predicting pressure drop and heat transfer coefficients for condensing annular-mist flows usually rely on correlations based on data taken for adiabatic two-component flows. As long as the vapor velocity is not too high these correlations are many times sufficient. However, they do not give sufficiently accurate results for the high vapor velocity single-component condensing situations considered in this paper. It was the purpose of this investigation to present an integral analysis that accurately models the high vapor velocity, two-phase annular-mist condensing flow system previously described. Possible applications of the resulting model are the design of compact light-weight tube condensers for space Rankine cycles and external combustion Rankine engines which require very high heat transfer coefficients at the expense of pressure drops which are large compared with those which occur in other tube condenser systems, such as vapor refrigeration cycles.

Correspondence concerning this paper should be addressed to W. P. Goss at the University of Massachusetts, Amherst, Massachusetts 01002. M. R. Berry, Jr. is with the Food and Drug Administration, Cincinnati, Ohio.

ANALYSIS

The pressure drop in annular two-phase flow systems is affected by three factors—friction, momentum, and gravity. Soliman et al. (*1*), Andeen and Griffith (2), and Carpenter and Colburn (3) discuss the relative contribution of these factors to the two-phase pressure drop in condensing flows. Friction dominates at high and intermediate dynamic qualities (the ratio of vapor flow rate to total flow rate), while the contribution due to the momentum flux becomes increasingly important at high density ratios (liquid to vapor) and can dominate in the low quality region. The effect of gravity will naturally depend on the orientation of the system. However, as long as the vapor velocity is sufficiently higher than that necessary to maintain the annular-mist flow pattern, gravity effects are negligible for all but low qualities (*1*, 3 to 5).

Of utmost importance in determining the two-phase pressure drop and heat transfer characteristics in annular-mist flow is the ability to predict accurate wall and interfacial shear stresses. Analytical predictions of these shear stresses are complicated since the interaction of the slow moving liquid and the high speed gas results in interfacial wave characteristics which are not well understood. Several investigators have tried to avoid the problem of determining wall and interfacial shear stresses by defining equivalent friction factors in these analyses which are de-

termined in a variety of ways (*6* to *9*).

The theoretical model developed for this investigation is that of a high-speed, pure fluid in a saturated gaseous state which is introduced into a tube which is externally cooled. The inlet gas will condense into a radially symmetric, slow-moving, thin annular film on the tube wall. Due to the shearing action of the high-speed gas, travelling waves will form at the gas-liquid interface, and eventually the gas begins to shear off the wave peaks. For high vapor velocity situations, this usually occurs quite close to the inlet. The liquid entrained in this manner is carried along in the gas and subsequently redeposited on the wavy liquid film. This process of liquid particle interchange continues up to the point where complete condensation occurs. The flow pattern is shown in Figure 1. In actuality, the film is much smaller than that shown and usually has many waves with amplitudes larger than the bulk film itself. Also, there are probably some entrained vapor bubbles in the film and the waves.

A complete analytical description of the flow must include the unsteady behavior of the waves at the liquid-vapor interface and the accompanying mass transfer across the interface due to both the macroscopic particle interchange and molecular condensation. Since it is not feasible at this time to include a wavy interfacial region, an analysis is presented which attempts to account for the wavy interface *without actually analyzing the interface itself*. The analysis is based on a time-averaged annular liquid film with a smooth gas-liquid interface. The interfacial waves affect the mass, momentum, and energy transfer mechanisms between the core and the annulus and are included in the following ways:

1. Mass Transfer: An entrainment correlation which predicts the amount of entrained liquid flowing in the gaseous core is employed.

2. Momentum Transfer: This effect must be determined at both the interface and the wall. The high-velocity, entrainment-laden gas core tends to drag the liquid annulus along while the rigid tube wall tends to retard it. Therefore, effective interfacial and wall shear stresses are included at the gas-liquid interface and the tube wall, respectively.

3. Energy Transfer: The energy transferred at the liquid-gas interface is related to both the mass and the momentum transfer through the coupling of the basic equations.

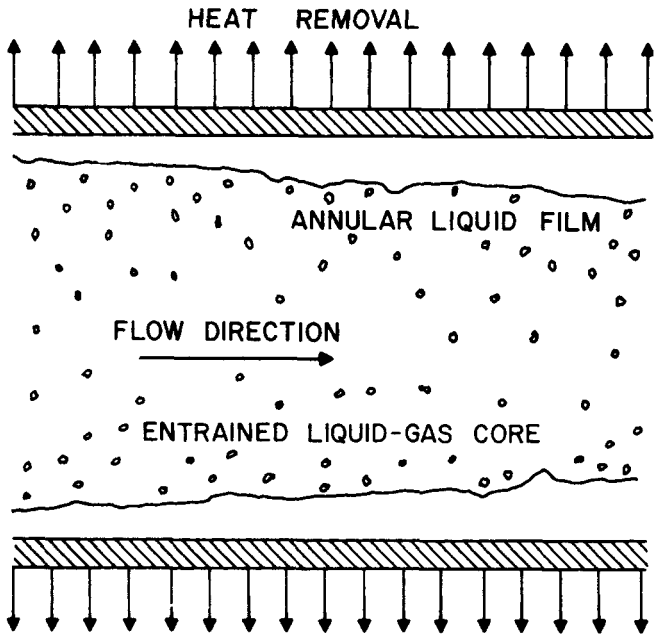

Fig. 1. Actual two-phase, annular-mist flow pattern.

The inclusion of the interfacial effects in the above manner reduces the analysis of a two-dimensional axisymmetric system with an entrained liquid-gas core region and an annular liquid film region. From this system, it is possible to start with the pure gas inlet conditions and the external cooling configuration and, subsequently, completely describe the flow at each point throughout the cylindrical tube up to the point of complete condensation.

In addition to the above discussion, certain simplifying assumptions are necessary to reduce the actual flow system to a theoretical model suitable for solution.

1. The core is homogeneous and its associated thermodynamic properties are assumed at the saturation conditions corresponding to the static pressure. A discussion of the validity of this assumption is given by Collier et al. (*10*). Radial variation in a property is allowed when passing from one phase to another.

2. In the liquid annulus, both radial and axial variations in the enthalpy are allowed.

3. The static pressure varies in the axial direction only.

4. The kinetic energy of the liquid flowing in the annulus is neglected.

5. The hydrodynamics of the liquid-vapor interface controls the entrainment mechanism. It is assumed that the flow of liquid crossing the liquid-vapor interface includes the combined effects of entrainment and condensation.

6. A constant ratio of local entrained liquid velocity to local gas velocity (S_E) is assumed throughout the core. From the available data on the entrainment slip ratio, the general opinion is that its value is near unity (*11*, *12*).

7. The wall heat flux and the wall temperature are known functions of axial position. This assumption is made in light of the existing experimental data. In actual design use, the heat flux would have to be determined from a correlation of the local condensing heat transfer coefficient, the tube geometry, and the external thermal conditions.

Applying fundamental laws to the control volumes illustrated in Figure 2 results in the following set of integral equations. At this point, it should be noted that integral techniques are ideally suited for idealized two-phase flow patterns. The possibility of averaging over different portions of the flow pattern readily allows the inclusion of a dispersed phase and/or separated phases without knowing the exact empirical details of the flow pattern. The details of the derivations of the resulting integral equations are contained in (*13*).

Conservation of mass of the total flow yields

$$\frac{d}{dx}\left[\rho_{cc}\int_{\delta}^{R} u_G(R-y)dy\right] + \frac{d}{dx}\left[\rho_f\int_{0}^{\delta} u_L(R-y)dy\right] = 0. \quad (1)$$

Newton's second law applied to the total flow yields

$$\frac{-R^2}{2}\frac{dP}{dx} - R\tau_\omega = \frac{d}{dx}\left[\rho_f\int_{0}^{\delta} u_L^2\,(R-y)dy\right] + \frac{d}{dx}\left[\rho_{cm}\int_{\delta}^{R} u_G^2\,(R-y)dy\right] \quad (2)$$

Newton's second law applied to the liquid annulus yields

$$\tau_I(R-\delta) - \delta\left(R-\frac{\delta}{2}\right)\frac{dP}{dx} - \tau_\omega R$$

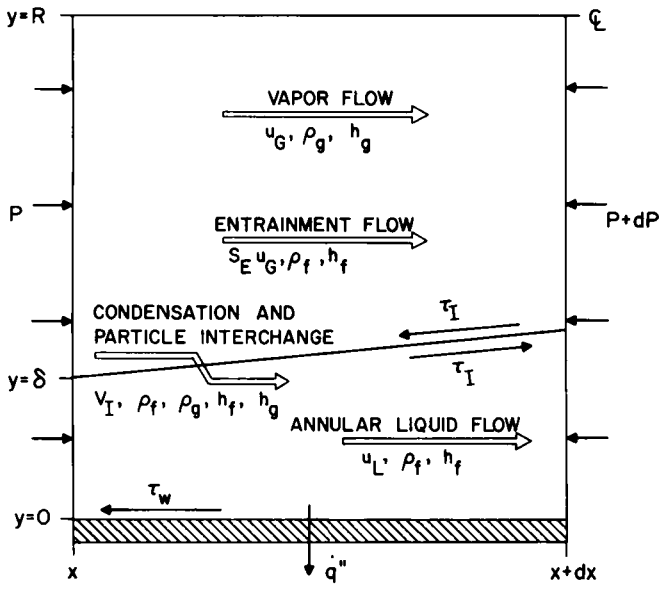

Fig. 2. Control volumes for the theoretical system.

$$= \frac{d}{dx}\left[\rho_f \int_0^\delta u_L^2 (R-y)dy\right] - V_I \frac{d}{dx}\left[\rho_f \int_0^\delta u_L (R-y)dy\right] \quad (3)$$

and applying the conservation of energy to the total flow yields

$$\frac{d}{dx}\left[\rho_c h_c \int_\delta^R u_G (R-y)dy\right] + \frac{d}{dx}\left[\rho_{cE} \int_\delta^R \frac{u_G^3}{2}(R-y)dy\right] + \frac{d}{dx}\left[\rho_f \int_0^\delta u_L h_L (R-y)dy\right] + R\,q'' = 0 \quad (4)$$

where the effective core densities are defined as

$$\rho_{cc} \equiv \alpha\rho_g + (1-\alpha)\, S_E \rho_f \quad (5)$$

$$\rho_{cm} \equiv \alpha\rho_g + (1-\alpha)\, S_E^2 \rho_f \quad (6)$$

$$\rho_{cE} \equiv \alpha\rho_g + (1-\alpha)\, S_E^3 \rho_f \quad (7)$$

and

$$\rho_c h_c \equiv \alpha\rho_g h_g + (1-\alpha)\, S_E \rho_f h_f \quad (8)$$

The above equations form a set of independent integral equations which must be solved simultaneously to describe the flow system.

There are various methods of solving these integral equations, all of which involve assuming suitable profiles in the radial direction and integrating these profiles, thus reducing the integral equations to ordinary differential equations. Good results may be obtained from integral equations when the boundary conditions are complex by assuming algebraically simple profiles and employing empirical or semi-empirical relations to satisfy the complex boundary conditions. This technique has been used quite successfully for turbulent, free convection flows (*14*). Due to the complexity of the boundary conditions that exist at the vapor-liquid interface for the two-phase, annular-mist flow system and also to the limited information available on velocity and temperature profiles, a similar technique is used in this analysis. The following steps are taken to reduce the set of integral equations into a set of four non-linear, first-order, ordinary differential equations with primary dependent variables V_I, V_{cl}, δ, and P and independent variable x:

1. Employ empirical or semi-empirical correlations for the wall shear stress, the interfacial shear stress, and the entrainment flow rate in terms of the dependent variables.
2. Assume velocity and enthalpy profiles for the core and annular liquid regions in terms of the dependent variables.
3. Perform the necessary integration and differentiation to reduce the equations to a form suitable for solving by numerical techniques.

Entrainment Correlation

The majority of the available correlations (*15* to *17*) are based on two-phase, annular-mist flow data of two components flowing adiabatically in a tube, usually air and water. Data taken at equilibrium conditions or when the entrainment rate equals the redisposition rate may be quite different from that which would occur in condensing flows of a single component when equilibrium conditions are highly unlikely. Due to the scatter in the available entrainment correlations and the question of applying air-water data taken under adiabatic conditions to condensing flows, a modification of the approximate correlation presented by Goss (*18*) will be used in this analysis. The correlation (Figure 3) is based on experimental data (*19*) from two-phase annular-mist flow of condensing steam and is given by the following expressions:

$$\theta = k[(1-a_1)t - a_2 t^2 - a_3 t^3 - a_4 t^4] \quad (9)$$

$$X = 2kt - \theta \quad (10)$$

where

$$k = 0.707107 \qquad a_3 = -2.246910\gamma$$
$$a_1 = 0.638377\gamma \qquad a_4 = 0.794244\gamma$$
$$a_2 = 1.137108\gamma$$

Essentially, Equations (9) and (10) express in parametric form the relationship between the total dynamic quality θ and the entrainment dynamic quality X. The parametric variable t is just used in determining values of X from values of θ. The only true correlation variable is γ which allows variation in the amount of entrained liquid in the core. Decreasing γ increases the amount of entrained liquid (Figure 3). When $\gamma = 0$, the two-phase flow would be in the homogeneous, mist flow regime. Since the core void fraction rather than the entrainment dynamic quality is needed in the analysis, the following expression which relates α to X was used:

$$\alpha = \frac{X\beta S_E}{1 + X\beta S_E - X} \quad (11)$$

Wall Shear Stress

The wall shear stress correlation used in this analysis is the semi-empirical correlation of Kammula (*20*) with slight modifications. The equations normally used to predict the velocity distributions and eddy viscosities in single-phase flow are adapted to fit condensing annular-mist flows with high interfacial drag by including a term which accounts for the interfacial shear stress and mass transfer. The procedure involves assuming a value for the wall shear stress and numerically integrating across the liquid film to determine the resulting flow rate. An iteration procedure is used to adjust the wall shear stress until the actual liquid film flow rate is attained. The liquid film flow rate is given by the expression

$$W_L = \pi D \mu_L \int_0^{\delta^+} \left[1 + \frac{2\,\delta/D}{\delta^+} y^+\right] \cdot$$

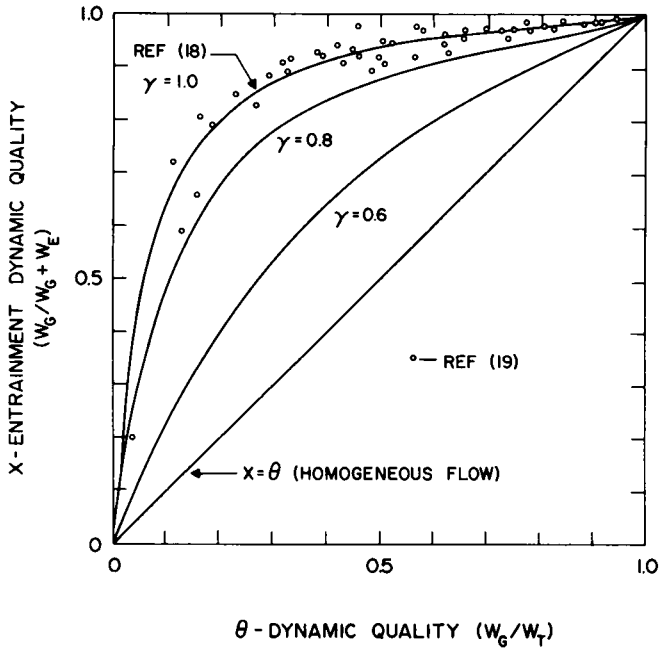

Fig. 3. Entrainment correlation.

$$\int_0^{y^+} \frac{\tau/\tau_\omega}{1+\frac{1}{2}\left[-1+\sqrt{1+4\frac{\tau}{\tau_\omega}K^2\eta^2\left[1-\exp(-\eta/A^+)\right]^2}\right]}\,d\eta dy^+ \qquad (12)$$

where K is the von Karman constant modified for annular-mist flow and A^+ is the van Driest turbulent damping constant which has a value of 26 for fully developed turbulent flow. The shear stress distribution is given by

$$\frac{\tau}{\tau_\omega}=\frac{R}{R-y}\left[1-\left(\frac{2R-y}{2R-\delta}\right)\frac{y}{\delta}\left[1-\frac{\tau_I}{\tau_\omega}\left(\frac{R-\delta}{R}\right)\right]\right] \qquad (13)$$

Kammula (*20*) suggests several correlations for obtaining the modified von Karman constant K as a function of other system properties. Unfortunately, these correlations are based on only one set of data, that of Hilding (*21*). It was found from the present investigation that the expressions which correlate more of the data with which this analysis will be compared are given as follows:

$$\text{for } k_p \leq 28 \quad K = 0.4\,(1+k_p)^{1.43}$$
$$\text{for } k_p > 28 \quad K = 6.63\,(1+k_p)^{0.6} \qquad (14)$$

The variable k_p which is the square root of the ratio of the vapor to liquid momentum fluxes is a function of the primary dependent variables.

Interfacial Shear Stress

The interfacial shear stress correlation used in this analysis is one proposed by the authors (*22*) for the condensing annular-mist flow of steam:

$$\text{for } 1.0 > \theta > 0.745 \quad \frac{\tau_I}{\tau_\omega}=\frac{2.0\theta^{0.589}-1}{\theta}$$
$$\text{for } 0.745 \geq \theta > 0.1 \quad \frac{\tau_I}{\tau_\omega}=\frac{1.735\theta^{0.111}-1}{\theta} \qquad (15)$$

These expressions are used as an input to the wall shear stress correlation, Equation (13). Once the wall shear stress is obtained, the interfacial shear stress is determined from Equation (15).

Velocity and Enthalpy Profiles

The velocity profile models to be used in this analysis are of the power-law type with the exponents left as independent variables. They are given by the following expressions:

$$u_L = V_I\,(y/\delta)^n \qquad (16)$$

$$u_G = V_I + (V_{cl}-V_I)\left[\frac{y-\delta}{R-\delta}\right]^m \qquad (17)$$

The assumed profiles satisfy the boundary conditions for velocity that

$$\text{at } y=0, \quad u_L = 0 \qquad (18)$$
$$\text{at } y=\delta, \quad u_L = u_G = V_I \qquad (19)$$

and,

$$\text{at } y=R, \quad u_G = V_{cl} \qquad (20)$$

Similarly, for the enthalpy profile, the following distribution is assumed for the liquid layer:

$$h_L = h_{fw} + (h_f - h_{fw})\,(y/\delta)^l \qquad (21)$$

The boundary conditions that are satisfied are that

$$\text{at } y=0, \quad h_L = h_{fw} \qquad (22)$$
$$\text{at } y=\delta, \quad h_L = h_f \qquad (23)$$

The assumed profiles allow the freedom of arbitrarily varying the shape of the profile as a function of the distance from the condenser entrance, thereby allowing developing flows and determining the effect of velocity and enthalpy distribution on the dependent variables.

Upon substitution of the assumed profiles into the set of integral equations and performing the integration in the radial direction followed by the differentiation with respect to the independent variable and with much rearranging and combining, the following set of nonlinear, first-order, ordinary differential equations written in index notation results:

$$a_{ij}\frac{d\psi_j}{dx} = b_i \qquad (24)$$

where

$$a_{ij} = a_{ij}\,(V_I, V_{cl}, \delta, P)$$
$$b_i = b_i\,(V_I, V_{cl}, \delta, P, x)$$
$$\psi_1 = V_I$$
$$\psi_2 = V_{cl}$$
$$\psi_3 = \delta$$
$$\psi_4 = P$$

The details of the simplification, along with the definitions of the coefficient matrix a_{ij} and the column matrix b_i, are given in (*13*). These equations may be solved by numerical techniques given the inlet conditions of pressure, total flow rate, and dynamic quality, and the external cooling configuration.

After simultaneously solving Equation (24) for the derivatives $d\psi_j/dx$ at an axial position X, Euler's method of numerical integration is then utilized to determine values of the dependent variables at a position $x + \Delta x$.

$$\psi_j|_{x+\Delta x} = \psi_j|_x + \left.\frac{d\psi_j}{dx}\right|_x \Delta x \qquad (25)$$

This procedure is repeated until the point of complete condensation occurs.

RESULTS AND DISCUSSION

Correlation with Experimental Data

The analytical results were compared with data from three experimental investigations' the data reported by Hilding (*12*), Taliaferro (*23*), and Goodykoontz and Dorsch (*24*). Hereafter, these data will be referred to as UCONN, VPI, and NASA, respectively. In each of these data, steam entered the condenser at a dynamic quality of greater than 96% and the measured inlet velocities indicated that all were well into the annular-mist flow regime. The parameters compared were the static pressure distributions and the average gas velocities. Typical static pressure distributions for the UCONN and VPI data are shown in Figures 4 and 5. Although not illustrated graphically, dynamic quality distributions and total condensation lengths compared extremely well in all cases where experimental data was available. For the particular cases tested, the dynamic quality remained approximately a linear function of axial position.

There are five main parameters which may be varied in the analysis. These are the three profile exponents m, n, and l, the entrainment slip ratio S_E, and the entrainment flow correlation variable γ. The UCONN data is, in general, for high-velocity condensing steam (entrance velocities in excess of 600 fps), and a variation in the shape of the velocity profiles alters the momentum contribution to the static pressure change more than for the slightly lower velocity VPI runs. A difference is seen in Figure 4 between the two-dimensional and one-dimensional (all exponents equal to zero) model for γ and S_E equal to unity.

Since the shape of the profiles seem to have relatively little effect on the analytical results, the profiles which

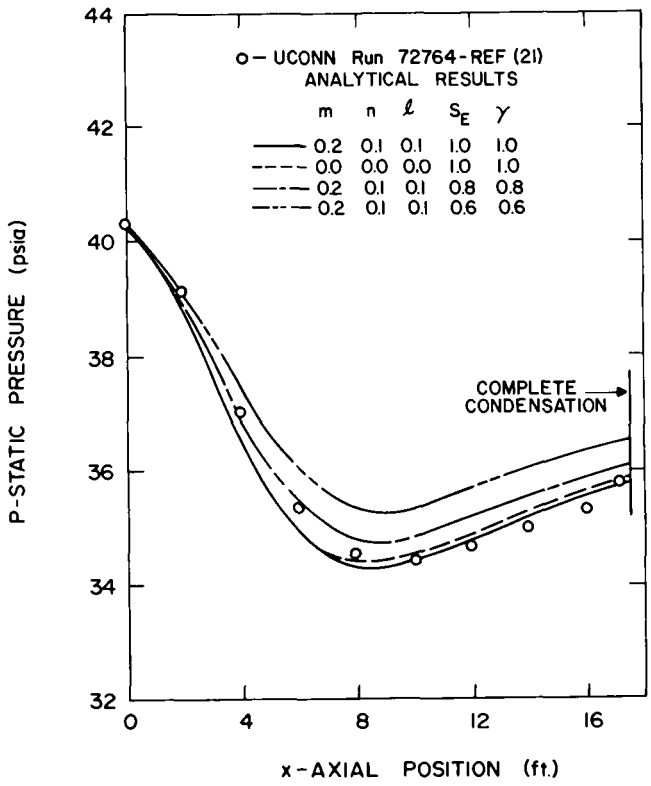

Fig. 4. Axial pressure distribution for UCONN Run 72764.

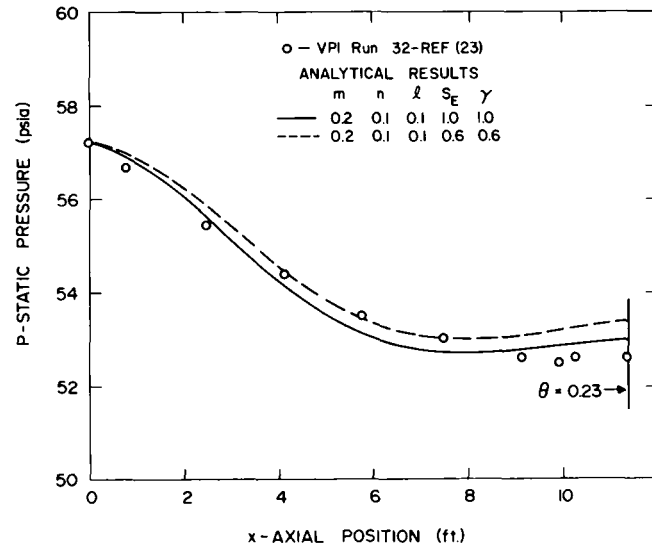

Fig. 5. Axial pressure distribution for VPI Run 32.

were used to obtain the majority of the results were a one-fifth velocity profile for the core and one-tenth profiles for the velocity and the enthalpy distributions in the annular liquid film. These profiles agree with the general trends reported in the rather limited experimental data available. Analytical solutions for developing type flows (that is, profiles whose exponents vary from zero at the entrance as a function of axial position) show no appreciable difference as compared to fully developed flows.

The effect of varying the entrainment slip ratio S_E and the entrainment correlation variable γ on the axial static pressure distribution is also illustrated in Figures 4 and 5. In all cases, a reduction in S_E and γ below a value of unity reduces the overall static pressure drop.

Ordinarily the axial static pressure distributions have the same general shapes. After some maximum static pressure drop, the frictional pressure drop becomes less than the pressure recovery due to the change in momentum. At that point, the static pressure begins to increase. In all cases, no appreciable deviations between the one- and two-dimensional results were observed until the pressure recovery, due to the change in momentum, significantly offsets the frictional pressure drop.

There are certain limitations to each of the sets of experimental data to which the analytical results are compared. All three experimental facilities were cooled externally by cooling water flowing in a coaxial tube. The UCONN facility consisted of a horizontal 1-1/16-in. I.D. copper tube. The system was not well instrumented in the entrance region. Of the six sets of UCONN data correlated, in three of the cases the analysis predicted overall pressure drops which were somewhat larger than those reported in (*21*).

The VPI facility consisted of a ¾-in. I.D. copper tube oriented for vertical downward flow. The data is subject to the limitation that complete condensation does not occur in the tube. Dynamic qualities at the exit ranged from 18 to 72%. The general agreement between analytical and experimental results shown in Figure 5 for the static pressure distribution is typical of the four sets of VPI data correlated for this investigation.

For the NASA data, a 0.293-in. I.D. copper tube oriented for vertical downward flow was used as a condenser. Figure 6 illustrates a comparison of analytical results and experimental data. In general, the NASA data can be categorized into two classes—those similar to run 172 in which the static pressure remained fairly constant or, as in run

171, where the overall pressure drop is quite large. Runs 171 and 172 were chosen as examples since they are actually quite similar runs. At the entrance for both runs the dynamic quality, the total steam flow rate, the static pressure, and, as a result, the vapor velocity and Reynolds number, were equal. The difference was that the coolant flow rate for run 172 was approximately 65% higher. The analytical results repeatedly predicted too large a pressure drop for the small pressure drop runs and vice versa, as illustrated in Figure 6. The inlet region of the NASA condenser was not completely instrumented, and accurate inlet conditions were difficult to obtain. Also, it should be emphasized that even though the flow parameters lie well within the region normally observed as the annular-mist flow regime, no indication was made as to the flow pattern obtained during the actual runs. Furthermore, some of the NASA data was subject to pressure fluctuations which may have been due to the presence of the boiler and superheater in the condensation loop.

Figure 7 illustrates a comparison of analytical results and experimental data for mass average gas velocity for UCONN run 72764. The results agree with the trend of the data. The major problem with this comparison is that the accuracy of the present methods for measuring gas velocities in two-phase, annular-mist flows is not known. Also shown are the predicted average gas velocities for

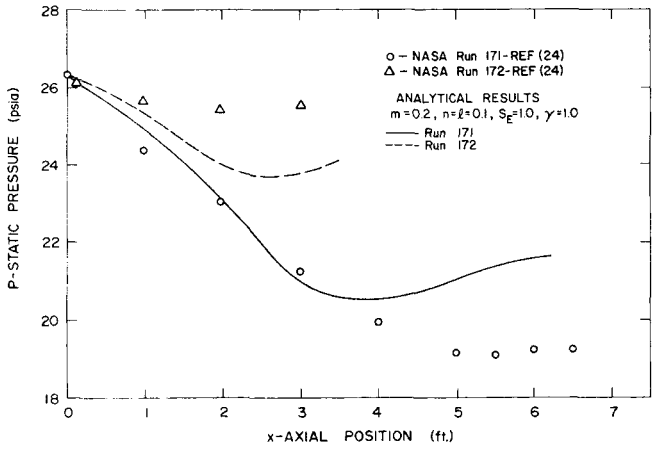

Fig. 6. Axial pressure distribution for NASA Runs 171 and 172.

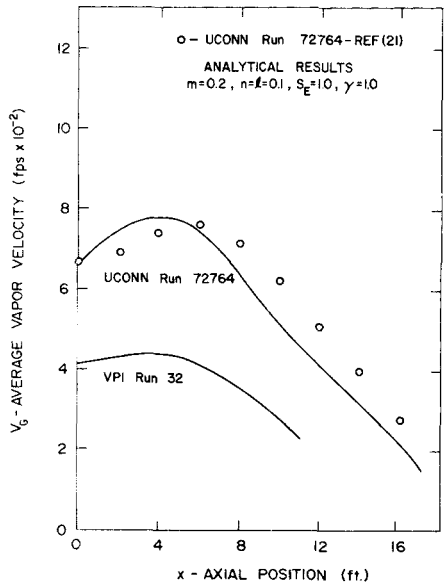

Fig. 7. Axial gas velocity distributions.

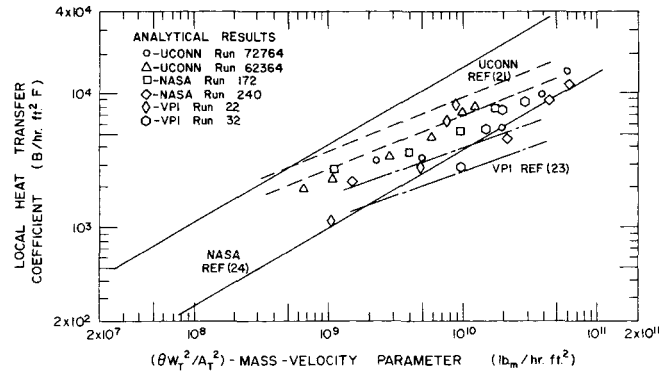

Fig. 8. Heat transfer correlations.

the VPI data which are considered as relatively low-velocity runs. Variations of the profile exponents or the entrainment parameters (S_E and γ) have a negligible effect on the average gas velocities.

Other trends noted were that the annular liquid layer thickness increased sharply near the entrance and also as the point of complete condensation was approached, while increasing at a lesser rate for intermediate positions. In general, the average liquid layer velocity approached a maximum (never exceeding 2 ft./sec.) in this intermediate region.

Heat Transfer Results

Normally in the design of condensers, only the external thermal environment and the vapor entrance conditions are specified. Therefore, energy removed from the condenser in the form of heat must be determined with the aid of a local condensing heat transfer coefficient correlation. Figure 8 compares a representation of the local heat transfer coefficients obtained analytically from the model used in this paper with experimental trends from the UCONN (*21*), VPI (*23*), and NASA (*24*) data. All of the UCONN experimental data (not shown) can be bracketed by the dashed lines, the VPI data with the occasionally dashed lines, and the NASA data by the solid lines.

The correlation shown is basically one of the local heat transfer coefficient versus the dynamic quality and was proposed by Goodykoontz and Dorsch (*24*). The analytical results (shown in Figure 8) exhibit similar trends and suggest the use of this correlation for actual design applications of the analytical model presented here. It should be noted that Figure 8 indicates the increase by one or two orders of magnitude in the heat transfer coefficient that is possible with high vapor velocity tube condensers. Likewise, the previous figures on the axial pressure distributions indicate the pressure drops which require additional pumping requirements.

The Effect of Varying the Slip Ratio and the Entrainment Correlation

The effect of simultaneously varying the entrainment slip S_E and the entrainment correlation variable γ on the static pressure distributions has been illustrated in Figures 4 and 5. In all cases, S_E and γ are equal and decreasing them below unity tends to decrease the overall static pressure drop. This result is a combination of two factors. First, decreasing the entrainment slip ratio decreases the velocity of the entrained liquid particles and, therefore, alters the contribution of the entrained liquid momentum change to the static pressure drop. Secondly, decreasing the entrainment correlation variable increases the entrainment flow rate which reduces the amount of liquid flowing

in the annular liquid film which in turn affects the wall shear stress distribution. In addition to the direct effect of the wall shear stress on the pressure drop, the increased entrainment flow rate also alters the momentum pressure drop since the additional entrainment flow has effectively been moved from the relatively slow moving annular film into the high-velocity core. Of the two effects, the second effect (that is, that effect of increased entrainment flow rate) proved to account for about 90% of the variation of the static pressure drop as shown in Figure 9 for UCONN run 72764.

Based on the above results, it appears that the amount of liquid flowing as entrained particles in the gaseous core has a significant influence on the prediction of the overall pressure drop (and likewise condensing heat transfer coefficients) for two-phase, annular-mist flow systems, whereas the relative velocity of the entrained particles S_E has much less of an effect on the results.

CONCLUSIONS AND RECOMMENDATIONS

In this investigation of the two-phase, annular-mist flow of a condensing vapor, the following significant conclusions are drawn.

1. The integral analysis presented indicates the general applicability of integral techniques to handle two-phase flow models, especially when there is a dispersed phase. The use of integral models allows some insight into the complex mechanisms and interactions which are occurring, without requiring the detailed empirical information necessary for the application of partial differential equation/finite difference techniques.

2. The integral analysis assumes velocity and enthalpy profiles of the power-law type. Varying the profile shapes has a negligible effect on the dynamic quality and static pressure distributions at all except high vapor velocities.

3. The analysis accounts for the slip between the entrained particles and the vapor in the gas core. A constant entrainment slip ratio S_E is assumed. Reducing the ratio below unity has an effect on the static pressure drop. The effect, however, is comparatively small.

4. Due to the lack of entrainment flow rate data available for two-phase, annular-mist, condensing flows, a variable entrainment correlation is included in the analysis. Changing the entrainment correlation variable γ influences the amount of liquid entrained as particles in the core. Increasing the entrainment flow rate significantly decreases the static pressure drop.

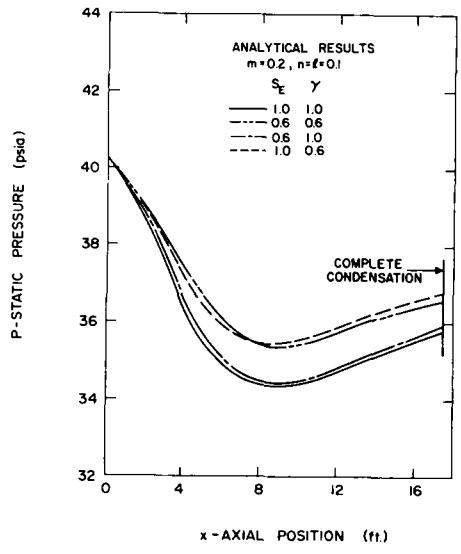

Fig. 9. Effects of S_E and γ on the pressure distributions for UCONN Run 72764.

5. More accurate and extensive experimental data for annular-mist condensing flows are needed before the correlations used in this analysis can be improved upon by both improved accuracy and a reduced number of correlation variables. Specifically, improved experimental techniques are needed for measuring vapor and liquid film velocity, temperature distributions, and entrainment flow rates in both the radial and axial direction for a high vapor velocity, two-phase, annular-mist condensing flow system.

ACKNOWLEDGMENTS

This study was carried out under the sponsorship of the Department of Mechanical Engineering, Virginia Polytechnic Institute and State University, and represents a portion of the Doctoral thesis of M. R. Berry, Jr. (*13*). The authors wish to acknowledge the support of this research by The Ethyl Corporation's Fellowship program and National Aeronautics and Space Administration under Grant NGR 47-004-006.

NOTATION

h = enthalpy, $B/lb._m$
k_p = square root of the ratio of the vapor to the liquid momentum fluxes, $(\rho_g V_G^2/\rho_f V_L^2)^{1/2}$
P = static pressure, lb./sq.in.abs.
$\dot{q}''$ = total radial heat transfer rate per unit surface area of the condensing tube, B/sq.ft. sec.
R = radius of constant area duct, ft.
S_E = entrainment slip ratio, V_E/V_G
T = temperature, F
t = nondimensional parametric variable in the entrainment correlation
u = local velocity in the axial direction, ft./sec.
V = velocity at a specific point or average velocity, ft./sec.
W = flow rate, $lb._m$/hr.
X = entrainment dynamic quality
x = distance from the tube entrance in the axial direction, ft.
Δx = increment in the axial direction, ft.
y = distance from the tube wall in the radial direction, ft.
α = core void fraction
β = ratio of the liquid to the vapor density
γ = variable in the entrainment correlation
δ = time-averaged thickness of the annular liquid film, ft.
θ = dynamic quality
μ = dynamic viscosity, $lb._f$sec/sq.ft.
ψ_j = column matrix defined by Equations (24)
ρ = density, $lb._m$/cu.ft.
τ = shear stress, $lb._f$/sq.ft.

Subscripts and Superscript

c = core
cl = centerline
f = liquid at saturation conditions
G = gas, vapor
g = vapor at saturation conditions
I = interface between the gaseous core and the annular liquid film
L = liquid in the annular film
T = total
w = wall
$^+$ = dimensionless quantity used in the wall shear stress correlation (quantity times $\sqrt{\tau_w \rho_f / g_c / \mu_L}$)

LITERATURE CITED

1. Soliman, M., J. R. Schuster, and P. J. Berenson, "A General Heat Transfer Correlation for Annular Flow Condensation," A.S.M.E. Paper No. 67-WA/HT-12 (1967).
2. Andeen, G. D., and P. Griffith, "Momentum Flux in Two-Phase Flow," A.S.M.E. Paper No. 67-HT-32 (1967).
3. Carpenter, E. F., and A. P. Colburn, "The Effect of Vapor Velocity on Condensation Inside Tubes," Proceedings of the General Discussion on Heat Transfer, Inst. Mech. Engr. and A.S.M.E., p. 20 (1951).
4. Kunz, H. R., "Theoretical Study of Heat Transfer for Annular Two-Phase Flow," Ph.D. thesis, Rensselaer Polytechnic Inst., Troy, N. Y. (1966).
5. Pletcher, R. H., and H. N. McManus, Jr., "An Analytic Study of Film Behavior in Horizontal Annular Two-Phase Flow," Cornell Univ., Ithaca, N. Y. (1965).
6. Hoffman, E. J., "Pressure Drop in Condensation," A.S.M.E. Paper No. 68-WA/HT-28 (1968).
7. Wrobel, J. R., and H. N. McManus, Jr., "An Analytic Study of Film Depth, Wave Height, and Pressure Drop in Annular Two-Phase Flow," Dev. in Mechanics, Vol. 1, Plenum Press, N. Y. (1961).
8. Wallis, G. B., "Use of the Reynolds Flux Concept for Analysing One-Dimensional Two-Phase Flow, Part II—Applications to Two-Phase Flow," *Intern. J. Heat Mass Transfer*, **11**, 459 (1968).
9. Chien, S. F., and W. Ibele, "Pressure Drop and Liquid Film Thickness of Two-Phase Annular and Annular-Mist Flows," *Trans. A.S.M.E., J. Heat Transfer*, **86**, 89 (1964).
10. Collier, J. G., P. M. C. Lacey, and D. J. Pulling, "Heat Transfer to Two-Phase Gas-Liquid Systems, Part II. Further Data on Steam/Water Mixtures in the Liquid Dispersed Region in an Annulus," *Trans. Inst. Chem. Engrs.*, **42**, T127 (1964).
11. Magiros, P. G., and A. E. Dukler, "Entrainment and Pressure Drop in Concurrent Gas-Liquid Flow—II. Liquid Property and Momentum Effects," Developments in Mechanics, Vol. 1, Plenum Press, N. Y. (1961).
12. Quandt, E. R., "Measurements of Some Basic Parameters in Two-Phase Annular Flow," *AIChE J.*, **11**, 311 (1965).
13. Berry, M. R., Jr., "An Integral Analysis of Two-Phase Annular-Mist Condensing Flows," Ph.D. thesis, Virginia Polytechnic Inst. and State Univ., Blacksburg (1970).
14. Eckert, E. R. G., and R. M. Drake, Heat and Mass Transfer, McGraw-Hill, N. Y. (1959).
15. Cousins, L. B., and G. F. Hewitt, "Liquid Phase Mass Transfer in Annular Two-Phase Flow: Droplet Deposition and Liquid Entrainment," United Kingdom Atomic Energy Authority, A.E.R.E.-R5657 (1968).
16. Paleev, I. I., and B. S. Filippovich, "Phenomena of Liquid Transfer in Two-Phase Dispersed Annular Flow," *Intern. J. Heat Mass Transfer*, **9**, 1089 (1966).
17. Farmer, R., P. Griffith, and W. M. Rohsenow, "Liquid Droplet Deposition in Two-Phase Flow," *Trans. A.S.M.E., J. Heat Transfer*, **92**, 587 (1970).
18. Goss, W. P., "Two-Phase, Annular-Mist Flow," Ph.D. thesis, Univ. Conn., Storrs (1967).
19. Hilding, W. E., and Staff, "Interim Progress Report on Heat Transfer Studies of Vapor Condensing at High Velocities in Straight Tubes," Report to N.A.S.A., Univ. Conn. (1965).
20. Kammula, K., "An Integral Technique for Prediction Wall and Interfacial Shear Stresses in Turbulent, Condensing, Annular-Mist Flow," M.S. thesis, Virginia Polytechnic Inst., Blacksburg (1970).
21. Hilding, W. E., et al., "An Analytical and Experimental Investigation of the Two-Phase Flow of a High Velocity Vapor Condensing in a Tube—Part II," Report to N.A.S.A., Univ. Conn. (1967).
22. Berry, M. R., Jr., and W. P. Goss, "Interfacial Shear Stress in Annular-Mist Condensing Flow," *Trans. ASME, J. of Heat Transfer*, **94**, 246 (1972).
23. Taliaferro, B., "A Study of Interfacial Waves and Heat Transfer for Turbulent Condensation in a Vertical Tube," M.S. thesis, Virginia Polytechnic Inst., Blacksburg (1970).
24. Goodykoontz, J. H., and R. G. Dorsch, "Local Heat-Transfer Coefficients and Static Pressures for Condensation of High-Velocity Steam Within a Tube," N.A.S.A. TN D-3953 (1967).

Manuscript received July 2, 1971; revision received March 15, 1972; paper accepted March 16, 1972.

Thermodynamics of Multi-Solute Adsorption from Dilute Liquid Solutions

C. J. RADKE and J. M. PRAUSNITZ

Department of Chemical Engineering
University of California, Berkeley, California 94720

The thermodynamics of ideal dilute solutions is applied toward establishing a method for predicting multi-solute adsorption using only data for single-solute adsorption from dilute liquid solution. The method is similar to that proposed by Myers and Prausnitz for adsorption of gas mixtures.

Experimental adsorption data for activated carbon at 25°C are reported for dilute aqueous solutions containing acetone and propionitrile, and *p*-chlorophenol and *p*-cresol. Calculated and experimental results are in excellent agreement for the first system and in fair agreement for the second system. It appears that the ideal dilute-solution theory for predicting multi-solute adsorption is most reliable for those systems where solute adsorption loading is moderate. When solute adsorption loading is large, the simplifying assumptions in the theory must be relaxed to allow for solute-solute interactions on the surface. The method presented here is simple to use and provides good approximations for engineering design.

Recent studies indicate the economic feasibility of purifying industrial and municipal waste waters by adsorption on activated carbon (*1*, *2*). Adsorption equilibria for mixtures of organic pollutants are required for design of these purification processes. To reduce experimental work, it is desirable to predict the adsorption of mixed organic solutes in dilute aqueous solution employing only experimental

C. J. Radke is at Pennsylvania State University, University Park, Pennsylvania 16802.